



**HAL**  
open science

## Tuning of organic heterojunction conductivity by the substituents' electronic effects in phthalocyanines for ambipolar gas sensors

Zeynel Şahin, Rita Meunier-Prest, Fabienne Dumoulin, Abhishek Kumar, Ümit Isci, Marcel Bouvet

### ► To cite this version:

Zeynel Şahin, Rita Meunier-Prest, Fabienne Dumoulin, Abhishek Kumar, Ümit Isci, et al.. Tuning of organic heterojunction conductivity by the substituents' electronic effects in phthalocyanines for ambipolar gas sensors. *Sensors and Actuators B: Chemical*, 2021, 332, pp.129505. 10.1016/j.snb.2021.129505 . hal-03364942

**HAL Id: hal-03364942**

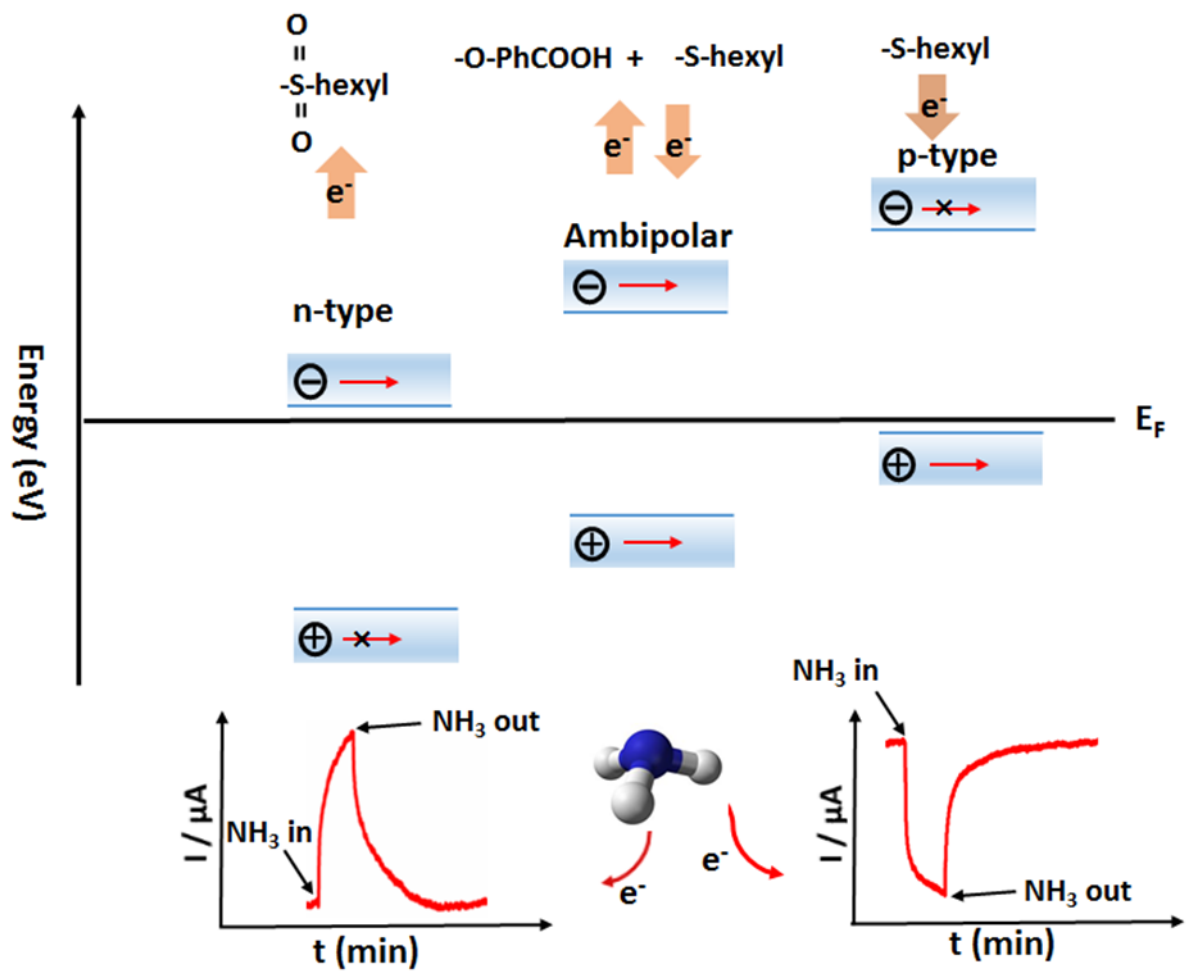
**<https://hal.science/hal-03364942>**

Submitted on 5 Oct 2021

**HAL** is a multi-disciplinary open access archive for the deposit and dissemination of scientific research documents, whether they are published or not. The documents may come from teaching and research institutions in France or abroad, or from public or private research centers.

L'archive ouverte pluridisciplinaire **HAL**, est destinée au dépôt et à la diffusion de documents scientifiques de niveau recherche, publiés ou non, émanant des établissements d'enseignement et de recherche français ou étrangers, des laboratoires publics ou privés.

Graphical abstract



## Tuning of organic heterojunction conductivity by the substituents' electronic effects in phthalocyanines for ambipolar gas sensors

Zeynel Şahin<sup>§</sup>, Rita Meunier-Prest<sup>†</sup>, Fabienne Dumoulin<sup>§‡</sup>, Abhishek Kumar<sup>†</sup>, Ümit İsci<sup>§\*</sup>, Marcel Bouvet<sup>†\*</sup>

<sup>§</sup>*Department of Chemistry, Gebze Technical University, 41400 Gebze – Kocaeli, Turkey  
(valid until 31 Dec 2019 for FD)*

<sup>†</sup>*Institut de Chimie Moléculaire de l'Université de Bourgogne (ICMUB), Université Bourgogne Franche-Comté, UMR CNRS 6302, 9 avenue A. Savary, F-21078 Dijon, France*

<sup>‡</sup>*Department of Medical Engineering, Acibadem Mehmet Ali Aydınlar University, Faculty of Engineering, Istanbul, Turkey*

---

**Abstract:** Exploiting organic heterojunction effects in electrical devices are an important strategy to improve the electrical conductivity, which can be utilized into improving the conductometric gas sensors performances. In this endeavor, the present article reports fabrication of organic heterostructures in a bilayer device configuration incorporating octa-substituted nickel phthalocyanines (NiPc) and radical lutetium bis-phthalocyanine (LuPc<sub>2</sub>) and investigates their sensing properties towards NH<sub>3</sub> vapor. NiPc having hexyl sulfanyl, hexyl sulfonyl and *p*-carboxyphenoxy moieties are synthesized, which electronic effects are electron donating, accepting and moderate accepting, respectively, also validated by cyclic voltammetry. The electronic effects of substituents in NiPc modulate the interfacial electrical conductivity and the type of the organic heterojunction formed. The electron acceptor and donor groups favor the formation of accumulation and accumulation/depletion heterojunctions, which are also correlated to negative and positive response towards NH<sub>3</sub>,

respectively. Among the studied heterojunction devices, the one based on hexyl sulfanyl groups, revealed the highest and the most stable response in 10-90 ppm of NH<sub>3</sub> and under variable relative humidity (rh) (10–70%). Interestingly, the bilayer device having *p*-carboxyphenoxy substituted NiPc, exhibited ambipolar behavior such that its p-type semiconducting nature is changed into n-type at higher rh values, also demonstrated by change in its negative response into positive towards NH<sub>3</sub>.

**KEYWORDS** molecular materials, phthalocyanine, conductometric transducer, heterojunction, gas sensor, ammonia

## 1. Introduction

Redox gas sensors are important electronic devices for air quality monitoring, industrial emission detection, biomedical analysis and hosts of other application areas. Conventionally, these sensors were used as a two-terminal and a three-terminal electrical device, such as resistors and Field-Effects Transistors (FET), respectively, in which a semiconducting material is used as a sensing layer. The working principle is based on modulation of charge carriers concentrations (electrons ( $e^-$ ) and holes ( $h^+$ )) in the semiconducting layer upon exposure to the redox gases environment, which is measured as a change in resistance or conductance depending on the associated transducer [1-3]. Majority of such sensors developed so far are based on metal oxides [4-9] like  $\text{SnO}_2$ ,  $\text{TiO}_2$ ,  $\text{ZnO}$ ,  $\text{MoO}_3$ ,  $\text{WO}_3$  and  $\text{Fe}_2\text{O}_3$ . These sensors demonstrated high sensitivity and low detection limit towards a range of redox gases including nitrogen dioxide ( $\text{NO}_2$ ) [10], ammonia ( $\text{NH}_3$ ) [11], ozone ( $\text{O}_3$ ) [12], sulfur dioxide ( $\text{SO}_2$ ) [13] and hydrogen sulfide ( $\text{H}_2\text{S}$ ) [14][15]. Many of these sensors have also attained commercial successes. Nonetheless, high performances of metal oxide based sensors are often met with certain limitations among which high costs associated with micro fabrications approach, poor selectivity, baseline signal drift and high temperature requirements are worth mentioning [15].

Organic semiconductors promise to be a suitable alternative, which are usually  $\pi$ -conjugated materials and have drawn a lot of interests in gas sensors development [16]. In the huge library of these conjugated materials, metal phthalocyanines (MPc) are one of the most extensively investigated molecular semiconductors, which are characterized by a macrocyclic structure, created by fusion of four isoindole subunits, forming a cavity in which different metal atoms can be placed. The structure and thin film properties of MPc materials are strongly correlated such that a subtle variation in the structure either by central metal atom substitution or by attaching electron withdrawing or donating substituents at the periphery

induces a huge change in the semiconducting properties. MPc materials manifest high chemical and thermal stability and solubility in wide ranges of organic and aqueous solvents, thus enabling their thin films processing by high vacuum and wet chemical processes. Except for those bearing long saturated substituents, MPc materials exhibited generally sufficiently high conductivity to be used in conductometric gas sensors. B. Bott et al. reported among the first such sensors based on conductivity change of PbPc film upon exposure to NO<sub>2</sub> [17,18]. The sensors exhibited enhancement in conductivity as expected for p-type PbPc film under exposure to electron acceptor gas and detected NO<sub>2</sub> down to 2 ppb at 150 °C working temperature. The sensors revealed fast response and recovery times (94 s and 154 s, respectively), which were further improved by thermal cycling at higher temperature. Chemiresistors based on different MPc (M: Cu, Ni, Co, Zn, Ni) and H<sub>2</sub>Pc were studied by A. C. Kummel et al. to detect a range of reducing gases, which also highlighted the gas sensing mechanism based on Lewis acidity of the metal center and binding enthalpy of the gas molecules [19,20]. The effect of central metal atoms and degree of fluorination in MPc was investigated on NH<sub>3</sub> sensing properties using chemiresistors based sensors [21]. The MPc with Co central metal and tetra-fluoro substitution showed highest response in 10-50 ppm NH<sub>3</sub> concentration range and fastest adsorption/desorption kinetics among CoPc, CuPc and ZnPc and their tetra and perfluorinated derivatives. Elsewhere, gas sensing performances of MPc materials in various devices were reviewed highlighting the thin films organizations and structural defects correlation with the electrical conductivity and finally their implications on sensing properties [22]. Despite showing high sensitivity and selectivity towards redox gases, MPc thin films based gas sensors suffer from prolonged response/recovery kinetics at room temperature associated with stronger chemisorption and diffusion of the gas molecules in the bulk [23]. Moreover, MPc thin films have poor organizations and charge transport mainly takes place by hopping process in discrete energy levels [24,25], which are often diminished

by extrinsic traps (water and oxygen) under extended exposure in ambient conditions, thus causing decrease in conductivity and lengthening of response and recovery times, particularly for n-type MPc [26]. Different approaches have been adopted to overcome these limitations such as use of a micro-heater to facilitate desorption [27], ultrathin films to prevent diffusion [28] and single crystal MPc films to enhance conductivity [29], but these methods are rather complex, expensive and present challenges to upscaling of sensors fabrication.

Another innovative approach is the use of MPc heterostructure in a suitable device design in which the associated organic heterojunction effects can be exploited to improve the conductivity and charges mobility. In organic heterojunction effects, opposite charge carriers ( $e^-$  and  $h^+$ ) are accumulated at the interface of the heterostructure because of workfunction differences of the semiconductors [30,31], filling the traps and making the charges hopping process much faster (interface conductivity increases up to 7-order from bulk). Moreover, in bilayer organic heterostructures, the dense packing of the molecules in the top layer acts as a kinetic barrier against diffusion of water and oxygen in the sublayer, which are traps for  $e^-$  carriers and destabilize the n-type organic semiconductors [32]. MPc materials are an ideal choice to realize organic heterostructures with desired properties because the workfunction, semiconducting polarity (n-type, and p-type) and carriers concentration of these macrocycles can be modulated by the electronic effects of peripheral substituents [33-35] and to a lesser extent by central metal atoms [36]. The potentiality of MPc heterostructures in redox gas sensors development has been investigated in the last decade, which is reviewed by us recently [37], highlighting the enhancement in the sensors performances like relative response (RR), sensitivity and response/recovery kinetics. These sensors were fabricated mainly in two device configurations, OFET [38-40] and Molecular Semiconductor - Doped Insulator heterojunctions (MSDI) [41]. MSDI consists of a bilayer of two organic semiconductors sequentially coated on interdigitated electrodes (Fig. 1), in which top layer has relatively

higher carriers density than sublayer, facilitating charge transport along the interface of the two layers. Different MSDI sensors were reported in recent years by us, starting from Cu(F<sub>16</sub>Pc)/LuPc<sub>2</sub> and CuPc/LuPc<sub>2</sub> (the first molecule is the sublayer and last is the top layer). In those devices, the former exhibited current increase under exposure to reducing gas like NH<sub>3</sub> while current decrease under oxidizing gas like O<sub>3</sub>, and *vice versa* for the latter device [42]. As shown for inorganic heterostructures [43,44], organic heterostructures also exhibit better sensing performances than resistors, which is reported in our recent studies on Cu(F<sub>16</sub>Pc)/LuPc<sub>2</sub> MSDI, demonstrating huge improvements in the NH<sub>3</sub> sensing properties (detection limit ~ 140 ppb) and stability in high relative humidity (rh) conditions from LuPc<sub>2</sub> chemiresistor [45]. In another such studies, M(Cl<sub>8</sub>Pc)/LuPc<sub>2</sub> (M: Co, Cu and Zn) MSDI revealed very high sensitivity and stability and displayed n-type, p-type and ambipolar behavior towards NH<sub>3</sub>, depending on the metal center in MPc [46]. Ambipolarity refers to a charge transport regime in which e<sup>-</sup> and h<sup>+</sup> concentrations are near equilibrium in device conduction channels and is rare in gas sensors. Ambipolar gas sensors have advantages of dual mode operations depending on bias polarity and multiplex sensing, using the same sensor [47], which can facilitate device miniaturizations [48].

In this endeavor, the present work aims to realize a sensitive, selective, stable and ambipolar MSDI device for NH<sub>3</sub> detection by tuning the charge transport in the device conduction channel through electronic effects of MPc substituents. Accordingly, a series of octa-substituted NiPc derivatives with electron-donating alkyl sulfanyl, electron-accepting alkylsulfonyl and combination of alkylsulfanyl and *p*-carboxyphenoxy (electron accepting) have been synthesized (Fig. 1). The structure, chemical purity and electronic properties of substituted NiPc derivatives have been assessed by optical and mass spectroscopies and electrochemical methods. These materials are then incorporated as sublayers by solution processing in MSDI devices in combination with LuPc<sub>2</sub> (Fig. 1) as top layer. The electrical

nature and the interfacial charges alignments of the MSDI devices have been evaluated by current-voltage; I(V) measurements. Finally, sensing performance of different MSDI devices have been investigated at variable NH<sub>3</sub> concentrations and wide range of rh variation.

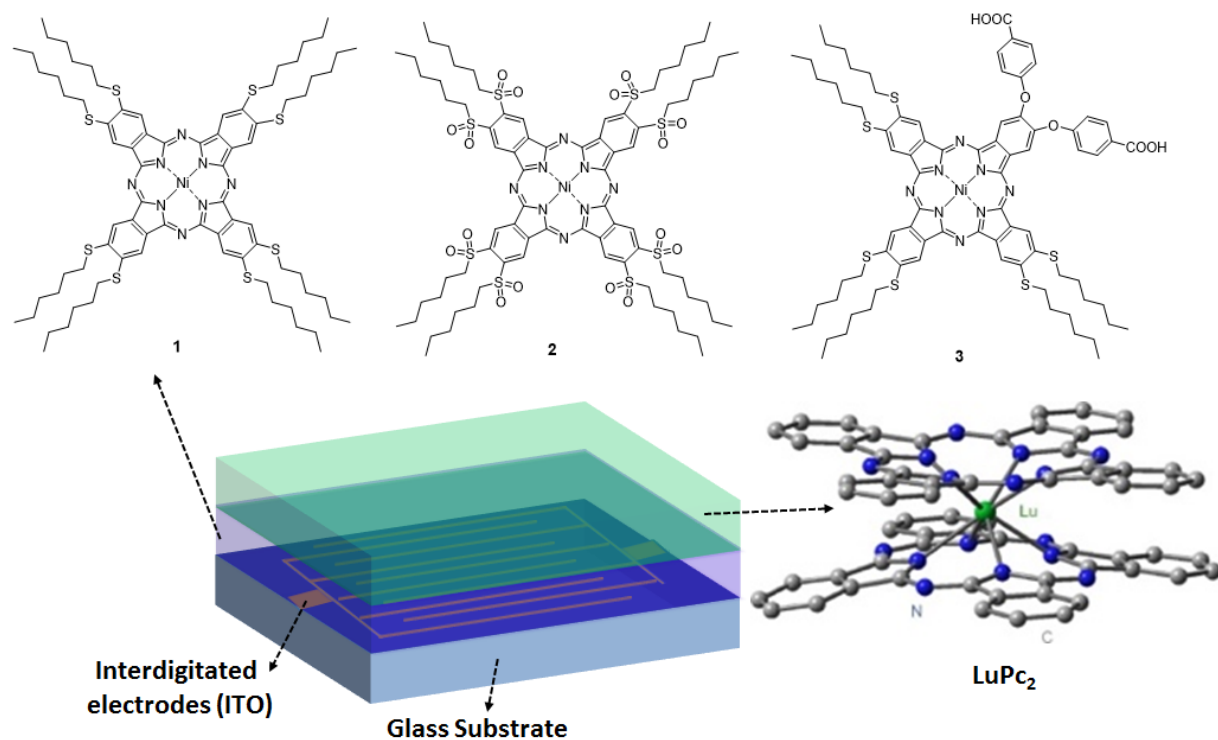


**Figure 1.** Chemical structure of the substituted nickel phthalocyanines **1-3** (top), LuPc<sub>2</sub> (bottom right) and schematic structure of the bilayer heterojunctions.

## 2. Experimental section

### 2.1. Materials and methods

4,5-Bis(hexylthio)phthalonitrile **4** and phthalocyanine **1** [49], 4,5-bis(hexylsulfonyl)-phthalonitrile **5** [50] and 4,5-bis(4-carboxymethylphenoxy)phthalonitrile [51] were prepared according to previously reported procedures. The lutetium bisphthalocyanine was synthesized according to a published procedure [52]. All other reagents and solvents were purchased as reagent grade from Aldrich, Fluka or Merck and used without further purification.

FT-IR spectra were recorded between 4000 and 650  $\text{cm}^{-1}$  using a PerkinElmer Spectrum 100 FT-IR spectrometer. Mass spectra were measured on a MALDI (matrix assisted laser desorption ionization) BRUKER Microflex LT (Bremen, Germany) using 1,8,9-anthracenetriol or 2,5-dihydroxybenzoic acid as the matrix. UV-visible electronic absorption spectra were recorded on a Shimadzu 2001 UV spectrophotometer. Raman spectral measurements were performed on a Renishaw inVia Raman microscope employing a 473 nm laser.

## 2.2. Syntheses.

**Synthesis of phthalocyanine 2.** Phthalonitrile **5** (1 g, 2.34 mmol) and  $\text{NiCl}_2$  (152 mg, 1.77 mmol) were heated overnight at 135 °C in a mixture o-dichlorobenzene/DMF (2/1) under argon, then the solvent was removed under reduced pressure. The blue solid residue was dissolved in dichloromethane, washed with water, and purified by chromatography on silica gel using a 100/1 mixture of  $\text{CH}_2\text{Cl}_2/\text{EtOH}$  as the eluent. Yield: 19 % (196 mg). MALDI-TOF-MS (DIT)  $m/z$ : 1754.199  $[\text{M}]^+$ ; calculated for  $\text{C}_{80}\text{H}_{112}\text{N}_8\text{NiO}_{16}\text{S}_8$ : 1754.532. FT-IR ( $\nu$   $\text{cm}^{-1}$ ) 3086, 2956, 2928, 2859, 1530, 1460, 1418, 1334, 1315, 1294, 1137, 1105, 1075, 921, 810, 756, 712.  $^1\text{H}$  NMR (500 MHz,  $\text{CDCl}_3$ )  $\delta$  ppm: 10.24 (8H, s, ArH), 4.04 (16H, s,  $\text{CH}_2$ ), 2.09 (16H, s,  $\text{CH}_2$ ), 1.54-1.25 (48H, s,  $\text{CH}_2$ ), 0.90 (24H, s,  $\text{CH}_3$ ).  $^{13}\text{C}$  NMR (125 MHz,  $\text{CDCl}_3$ );  $\delta$  ppm: 14.13, 22.56, 28.28, 31.48, 57.71, 128.77, 139.36, 142.03, 146.93. UV-Vis ( $\text{CHCl}_3$ ):  $\lambda_{\text{max}}$ , nm ( $\log \epsilon$ ) = 675 (5.5), 608 (4.7), 349 (5.0) nm.

**Synthesis of phthalocyanine 7.** A mixture of phthalonitrile **6** (208 mg, 0.49 mmol), phthalonitrile **4** (2.102 g, 5.83 mmol) and  $\text{NiCl}_2$  (409 mg, 3.16 mmol) was refluxed in a *n*-pentanol (8 mL) and 1,8-diazabicyclo[5.4.0]undec-7-ene (0.5 mL) under argon for 12 h. After cooling to room temperature, the reaction mixture was poured into ethanol (200 mL). The precipitate was separated from the supernatant and washed multiple times with ethanol. Phthalocyanine **7** was isolated by chromatography on silica gel using a mixture of

CH<sub>2</sub>Cl<sub>2</sub>:EtOH (100:1) as the eluent. Yield: 21 % (160 mg). MALDI-TOF-MS (DIT) m/z: 1566.544 [M]<sup>+</sup>; calculated for C<sub>84</sub>H<sub>100</sub>N<sub>8</sub>NiO<sub>6</sub>S<sub>6</sub>: 1566.098. FT-IR (ν, cm<sup>-1</sup>) 3056, 2956, 2927, 2856, 1718, 1598, 1505, 1434, 1420, 1265, 1122, 1164, 1095, 1074, 968, 894, 859, 894, 859, 736, 704. <sup>1</sup>H NMR (500 MHz, CD<sub>2</sub>Cl<sub>2</sub>) δ ppm: 7.73 (5H, s, ArH), 7.40-7.32 (4H, m, ArH), 6.61 (7H, s, ArH), 3.92 (6H, s, OCH<sub>3</sub>), 2.96-2.86 (8H, m, CH<sub>2</sub>), 1.78 (8H, s, CH<sub>2</sub>), 1.53 (8H, s, CH<sub>2</sub>), 1.40 (20H, s, CH<sub>2</sub>), 1.25 (14H, s, CH<sub>2</sub>), 0.98 (12H, s, CH<sub>3</sub>), 0.89 (6H, t, CH<sub>3</sub>). <sup>13</sup>C NMR (125 MHz, CD<sub>2</sub>Cl<sub>2</sub>) δ ppm: 13.95, 13.99, 14.03, 22.61, 22.71, 28.14, 28.52, 28.99, 29.18, 31.95, 32.69, 33.49, 33.80, 51.67, 114.06, 115.59, 116.67, 188.00, 124.38, 131.34, 131.60, 132.02, 137.96, 139.21, 140.12, 141.88, 143.20, 143.50, 146.43, 161.28, 165.86. UV-vis (CHCl<sub>3</sub>): λ<sub>max</sub>, nm (log ε): 695 (5.2), 664 (4.9), 325 (5.0).

**Synthesis of asymmetric phthalocyanine 3.** Phthalocyanine **7** (90 mg, 0.05 mmol) was dissolved in a THF/MeOH mixture (1:1, 10 mL) followed by addition of 2 ml of freshly prepared 1 M NaOH and stirring of the resulting mixture for 6 h in ambient condition. Another portion of 1 M NaOH solution (1 mL) was then added and the reaction mixture was stirred for an additional 18 h. HCl solution (2 M, 2 mL) was then added and the reaction mixture was poured into water. The resulting precipitate was filtered off and washed several times with hot acetone, chloroform and dichloromethane. Yield: 92% (81 mg). MALDI-TOF-MS (DIT) m/z: 1538.424 [M]<sup>+</sup>; calculated for C<sub>84</sub>H<sub>96</sub>N<sub>8</sub>NiO<sub>6</sub>S<sub>6</sub>: 1538.513. FT-IR (ν, cm<sup>-1</sup>) 3074, 2955, 2925, 2855, 2632, 2543, 1688, 1598, 1506, 1450, 1419, 1388, 1348, 1273, 1218, 1160, 1094, 1071, 968, 891, 851, 750, 726 cm<sup>-1</sup>. UV-vis (THF): λ<sub>max</sub>, nm (log ε): 691 (4.8), 663 (4.6), 322 (4.8).

### 2.3. Electrochemical studies.

All electrochemical experiments were performed with a PGSTAT302 N (Metrohm) potentiostat connected to a PC and the data collected were analyzed using the Nova® 2.1 Software. The experiments were performed in a conventional 3-electrode cell configuration employing Pt disk (1.6 mm in diameter), Pt wire and a saturated calomel electrode (SCE) as working, counter and reference electrodes, respectively. Cyclic voltammetry (CV) of **1-3** ( $2 \times 10^{-4}$  M) was conducted either in 0.1 M  $\text{CH}_2\text{Cl}_2 + \text{Et}_4\text{NBF}_4$  or MeCN +  $\text{Bu}_4\text{NPF}_6$  depending on the solubility of MPc. The working Pt disk was cleaned and activated by soaking for 10 min in KOH (2 M) followed by polishing with 0.1  $\mu\text{m}$  alumina powder and finally etched for 10 min in concentrated sulfuric acid (2 M). The electrode was then sonicated for 10 min in water, and then in absolute ethyl alcohol. All the electrochemical experiments were conducted in the absence of oxygen by bubbling argon in the solution for 10 min and maintaining the argon flow above the solution during the measurement time.

#### **2.4. Device and electrical measurements.**

Sensors were fabricated using a 1 x 1  $\text{cm}^2$  glass substrate over which Indium Tin Oxide (ITO) interdigitated electrodes (IDE) were lithographically patterned with a separation of 75  $\mu\text{m}$  between the electrodes. Over these glass substrates, films of **1**, **2** or **3** were drop casted at first using an ink prepared in organic solvents (details given in results and discussion part), followed by coating of 50 nm of thick film of LuPc<sub>2</sub>, using a PVD thermal evaporator (UNIVEX 250, Oerlikon, Germany) at a rate of 1  $\text{\AA} \cdot \text{s}^{-1}$ . The experimental setup used for electrical measurements and gas sensing was previously described [53]. The test bench consisted of different mass flow controllers, electronic valves and a test chamber which was connected with an ammonia source (commercial cylinder, Air Liquide, France; concentration 985 ppm in synthetic air) and a synthetic air (Air Liquide, France) for dilution. Desired concentrations of  $\text{NH}_3$  in the range of 1-90 ppm in the test chamber (8  $\text{cm}^3$ ) were obtained by controlling the flow in different fluidic lines, which were precisely controlled by a customized

homemade software. An additional fluidic line in the test bench was devoted for controlling the relative humidity in the test chamber, which was connected with an external humidity generator water tank, calibrated by a commercial humidity sensor (HMT-100, Vaisala, Finland). The sensing measurements were performed in a dynamic way, through alternate exposure / recovery cycles of 1 or 10 min / 4 or 40 min, respectively. These experiments were also carried out in the presence of variable relative humidity in the range of 10–70%.

### 3. Results and discussion

#### 3.1. Design and synthesis of materials

Our selection of MPc materials are motivated from the desired n-type, p-type and ambipolar transport in the bilayer organic heterojunction devices. In MSDI heterojunction devices, the polarity of charge transport is always determined by the semiconducting type of the sublayer because electrodes are embedded in it [42]. Thus, three different octa-substituted NiPc were synthesized to be incorporated as sublayer in the sensing device. NiPc like any other monocyclic MPc in unsubstituted form is a p-type semiconductor [54], which can become n-type or ambipolar in the presence of strong and moderate electron withdrawing substituents, respectively. The presence of an electron donating substituents make it more p-type by enhancing  $h^+$  charge carrier's density. Accordingly, NiPc symmetrically substituted with 8 donor n-hexyl sulfanyl ( $C_6H_{16}S-$ ), 8 acceptor n-hexyl sulfonyl ( $C_6H_{16}SO_2-$ ) and asymmetrically substituted with a combination of 6 donor hexyl sulfanyl and 2 moderate acceptor *p*-carboxyphenoxy groups were synthesized and are named as **1**, **2** and **3**, respectively hereinafter. For the synthesis of **1**, **2** and **3**, a common precursor is 4,5-bis-(hexylthio)-1,2-phthalonitrile (to be denoted as **4**), which were obtained by a base-catalyzed nucleophilic aromatic substitution reaction of 1, 2 -dichloro-phthalonitrile, as reported

previously [49]. As shown in Fig. 2, preparation of **1** was performed by using cyclotetramerization of **4** in the presence of NiCl<sub>2</sub> in a pentanol/1,8-diazabicyclo[5.4.0]undec-7-ene (DBU) mixture. The phthalonitrile precursor **5** of compound **2** was synthesized by the oxidation of **4** in H<sub>2</sub>O<sub>2</sub> into hexyl-sulfone, which was subsequently cyclotetramerized in the presence of NiCl<sub>2</sub> in dimethylformamide/*o*-dichlorobenzene (DMF/*o*-DCB) solution, forming **2**. The yield (19%) was in the range of our previous reports of the formation of the analogous Fe derivative [50]. In the synthesis of **2**, the specific use of a mixture of DMF/*o*-DCB is worth mentioning, because in the cyclotetramerization reaction common alcohol solvents act also as nucleophile on the sulfonyl functionality and degrade the phthalonitrile [55].

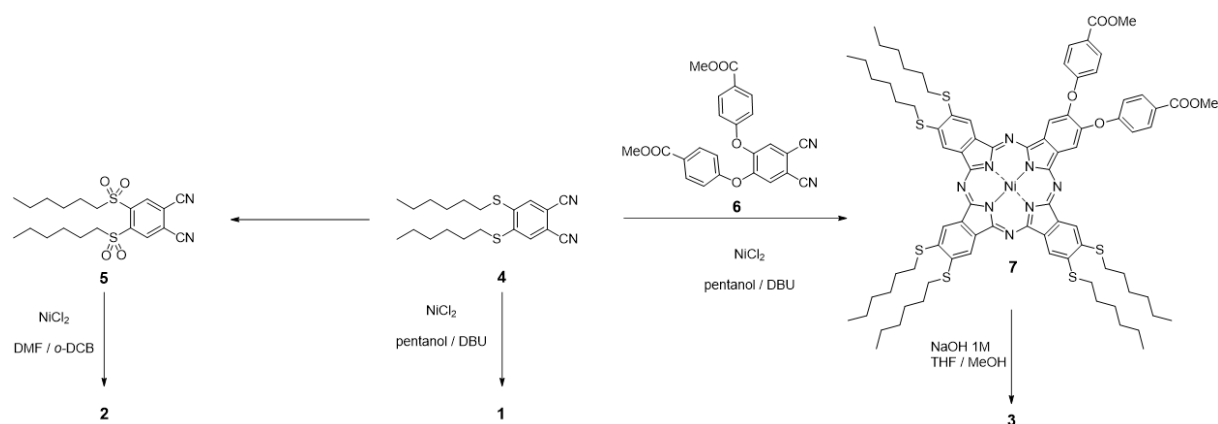


**Figure 2:** Synthesis of NiPc derivatives **1**, **2** and **3** from their phthalonitrile precursors.

To synthesize NiPc derivative **3**, phthalonitrile **4** was mixed with 4, 5-bis-(carboxyphenoxy)-1,2-phthalonitrile **6** to obtain at first an intermediate phthalocyanine **7**, which was subsequently hydrolyzed to get the final product [51]. As often for the synthesis of A3B asymmetric phthalocyanines, in order to limit the formation of undesirable asymmetric derivatives (A2B2, AB3 and B4) and obtain only a mixture of A3B and A4 (**7** and **1** here), a large excess (~12/1) of phthalonitrile A (**4** for this work) has been used. The reaction successfully gave a mixture of phthalocyanines **1** and **7**. It is worth to note that no transesterification was observed with the solvent during the formation of **7**. The mixture of

phthalocyanines was easily separated by column chromatography, **1** being first eluted as it is significantly less polar than **7**, which was hereafter recovered. The ester function of **7** was hydrolyzed by a solution of NaOH in a mixture of THF and methanol, giving the desired phthalocyanine **3** in excellent yield (92%). The phthalocyanines were characterized by  $^1\text{H}$  and  $^{13}\text{C}$  NMR except **3**, due to its amphiphilic structure, making it insoluble at the concentration requested for NMR recording in all deuterated solvents at our disposal (THF- $d_8$ , DMSO- $d_6$ ,  $\text{CDCl}_3$ ,  $\text{CD}_2\text{Cl}_2$ , pyridine- $d_5$ ,  $\text{CD}_3\text{OD}$ ). All these phthalocyanines were also characterized by UV-vis (Fig. S1) and FT-IR (Fig. S2) spectroscopies and MALDI mass spectrometry (Fig. S3), confirming the proposed structures and their purity.

For the top layer in the MSDI heterojunction, LuPc<sub>2</sub> was used because of its high conductivity originating from its radical nature, which is also indispensable for superior gas sensing response. Since during the sensor operation, only top layer of MSDI interacts with gas molecules, which either donate  $e^-$  or  $h^+$  in it. High carriers density ( $5 \times 10^{16} \text{ cm}^{-3}$ ) and low band gap (0.5 eV) of LuPc<sub>2</sub> [24,56] also facilitate faster charge transfer to the interface, which ultimately determines the device sensing performance. Moreover, LuPc<sub>2</sub> is thermally stable at high temperature, thus was deposited into thin films by vacuum sublimation over substituted NiPc derivatives. As shown in the SEM image of 50 nm thick LuPc<sub>2</sub> films (Fig. 3a), a dense morphology is observed, highlighting a compact molecular packing of the macrocycles. Such a dense packing of the top layer thin film in MSDI heterostructure acts as a kinetic barriers against oxygen and humidity diffusion into the sublayer and thus protects the sublayer from oxidation [26]. The thermal robustness of LuPc<sub>2</sub> was confirmed in the EDS measurements (Fig. 3b) because EDS peak associated with carbon (0.3 keV), nitrogen (0.4 keV) and lutetium (1.6 keV) can be clearly noticed in the spectrum.

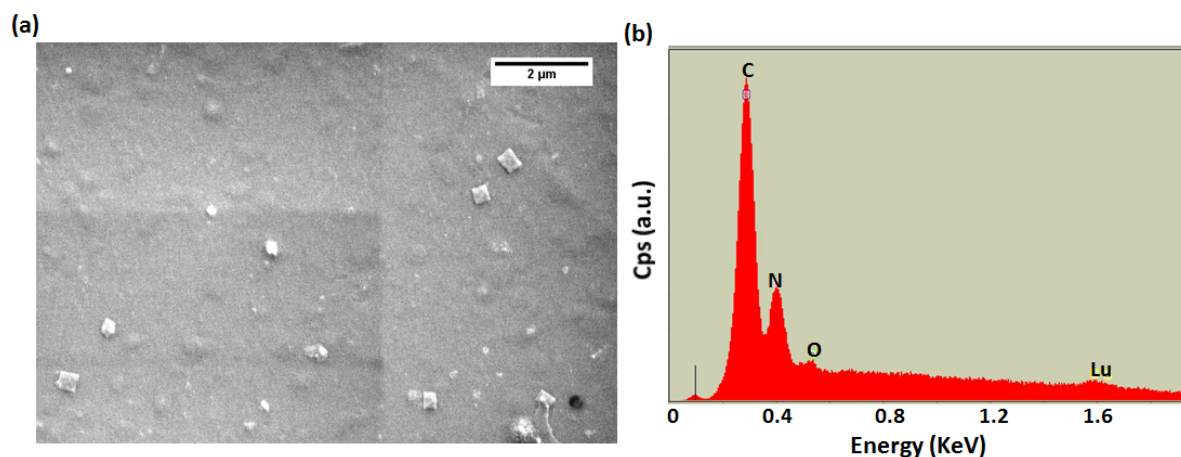


**Figure 3:** SEM image of 50 nm of LuPc<sub>2</sub> deposited on glass (a) and EDS of LuPc<sub>2</sub> film (b).

### 3.2. Electronic properties of NiPc derivatives: substituents effects

The nickel phthalocyanines **1-3** were studied by cyclic voltammetry either in CH<sub>2</sub>Cl<sub>2</sub> or in CH<sub>3</sub>CN depending on the solubility. The voltammograms exhibit two monoelectronic redox systems, one reduction ( $E_{\text{Red}}$ ) and one oxidation step ( $E_{\text{Ox}}$ ), as shown in Fig. 4a for **3**. The peak current increases linearly with the scan rate (Fig. 4b) in the range 0.02-0.2 V s<sup>-1</sup> and the difference between the anodic and cathodic peak is less than 30 mV, indicating that adsorption occurs. The potentials are reported in Table 1 as  $E_{\text{pc}}$  or  $E_{\text{pa}}$  for irreversible systems or as  $E_{1/2}$  for pseudo-reversible ones. Compared to those of **1**, the potential values  $E_{\text{Red}}$  and  $E_{\text{Ox}}$  of **2** are respectively shifted toward positive values by + 0.29 V and +0.11 V in CH<sub>2</sub>Cl<sub>2</sub> and + 0.44 V and + 0.31 V in CH<sub>3</sub>CN. These results are in accordance with those reported in the literature for metal-free phthalocyanine bearing eight peripheral octa-methylsulfanyl and octa-methylsulfonyl groups and for copper [57] and zinc complexes [58]. It confirms the strong electron withdrawing effect of hexyl sulfonyl groups as expected from their Hammett's constants [59]. The potential values of **3** are very close to those of **1**. The oxidation system of **3** appears 0.12 V lower than that of **1** whereas the reduction peak is shifted towards positive potentials by +0.13 V. This result shows a moderate electron-withdrawing character of the p-carboxylic-phenoxy substituents. It is in accordance with the observation of a n-type behavior

for the holmium bisphthalocyanine complex bearing sixteen phenoxy substituents [60], while unsubstituted rare earth bisphthalocyanine complexes are p-type materials. Here, the presence of  $-\text{CO}_2\text{H}$  moieties reinforces the electron-withdrawing character of the phenoxy groups, even though this effect remains low.

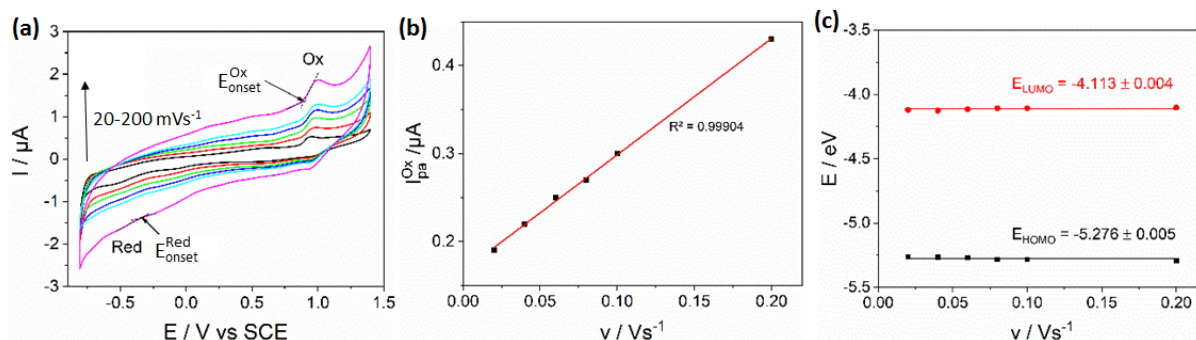


**Figure 4.** Cyclic voltammograms of **3** at  $2 \times 10^{-4}$  M in  $\text{CH}_3\text{CN} + \text{Bu}_4\text{NPF}_6$  0.1 M, on a Pt disk electrode (diameter 1.6 mm) at different scan rates (a), variation of the anodic peak current (b) and of  $E_{\text{HOMO}}$  and  $E_{\text{LUMO}}$  (c) with the scan rate.

Electrochemical potentials were used to evaluate the energy values of the frontier orbitals, HOMOs and LUMOs. The onset potential ( $E_{\text{ONSET}}$ ) defined as the potential at which the initial electron transfer from the HOMO, or to the LUMO, becomes visible on the cyclic voltammogram as a rise in anodic or cathodic current, respectively, is used [61,62]. The energy of HOMOs ( $E_{\text{HOMO}}$ ) and LUMOs ( $E_{\text{LUMO}}$ ) was determined from the  $E_{\text{ONSET}}$  values determined in solution versus SCE, as a reference electrode:

$$E_{\text{HOMO or LUMO}} = -(E_{\text{onset/SCE}}^{\text{Ox or Red}} + 4.4) \quad (1)$$

The presence of eight hexyl sulfonyl groups in **2** lowered  $E_{\text{HOMO}}$  and  $E_{\text{LUMO}}$ , whereas the substitution of two hexyl sulfanyl by two p-carboxyphenoxy groups induced a little decrease of both energy levels (Fig. S4). Notably, the nature of the substituents has little effect on the HOMO-LUMO gaps. It is worth noting that these gap values calculated from the onset

potentials are smaller than those calculated from  $E_{1/2}$ , but reflects more the electron transfers in the solid state, which are responsible for the electrical properties of the devices.

**Table 1.** Potentials of oxidation and reduction steps of a series of phthalocyanines determined by cyclic voltammetry vs SCE, and  $E_{\text{HOMO}}$  and  $E_{\text{LUMO}}$  deduced from Equation 1.

| Compound  | Solvent                         | $E_{\text{Red}}^{\circ}$ (V)     | $E_{\text{Ox}}^{\circ}$ (V)     | $E_{\text{onset}}^{\text{Red}}$<br>(V) | $E_{\text{onset}}^{\text{Ox}}$<br>(V) | LUMO<br>(eV)       | HOMO<br>(eV)       |
|---|---------------------------------|----------------------------------|---------------------------------|--|---------------------------------------|--------------------|--------------------|
| <b>1</b>  | CH <sub>2</sub> Cl <sub>2</sub> | -0.41 ( $E_{\text{pc}}$ )        | 1.09 ( $E_{\text{pa}}$ )        | -0.24                                  | 0.88                                  | -4.15              | -5.28              |
|   | MeCN <sup>a</sup>               | -0.65 ( $E_{\text{pc}}$ )        | 1.08 ( $E_{\text{pa}}$ )        | -0.44                                  | 0.83                                  | -3.96              | -5.23              |
| <b>2</b>  | CH <sub>2</sub> Cl <sub>2</sub> | -0.12 ( $E_{1/2}$ )              | 1.20 ( $E_{\text{pa}}$ )        | -0.03                                  | 1.05                                  | -4.37              | -5.45              |
|   | MeCN <sup>a</sup>               | -0.21 ( $E_{\text{pc}}$ )        | 1.39 ( $E_{\text{pa}}$ )        | 0.07                                   | 1.23                                  | -4.47              | -5.63              |
| <b>3</b>  | MeCN                            | -0.52 ( $E_{\text{pc}}$ )        | 0.96 ( $E_{1/2}$ )              | -0.29                                  | 0.88                                  | -4.11              | -5.28              |
| Cu(SC <sub>8</sub> H <sub>17</sub> ) <sub>8</sub> Pc [57] | CH <sub>2</sub> Cl <sub>2</sub> | -0.61 <sup>b</sup> ( $E_{1/2}$ ) | 1.24 <sup>b</sup> ( $E_{1/2}$ ) |  |                                       | -3.41 <sup>d</sup> | -5.26 <sup>d</sup> |
| Cu(SO <sub>2</sub> CH <sub>3</sub> ) <sub>8</sub> Pc [57] | CH <sub>2</sub> Cl <sub>2</sub> | 0.12 <sup>b</sup> ( $E_{1/2}$ )  | 1.73 <sup>b</sup> ( $E_{1/2}$ ) |  |                                       | -4.14 <sup>d</sup> | -5.77 <sup>d</sup> |
| Zn(SC <sub>8</sub> H <sub>17</sub> ) <sub>8</sub> Pc [63] | THF                             | -1.37 <sup>c</sup> ( $E_{1/2}$ ) | 0.14 <sup>c</sup> ( $E_{1/2}$ ) |  |                                       | -3.43 <sup>d</sup> | -4.94 <sup>d</sup> |
| Zn(SO <sub>2</sub> CH <sub>3</sub> ) <sub>8</sub> Pc [63] | CH <sub>2</sub> Cl <sub>2</sub> | -0.74 <sup>c</sup> ( $E_{1/2}$ ) | 0.88 <sup>c</sup> ( $E_{1/2}$ ) |  |                                       | -4.06 <sup>d</sup> | -5.68 <sup>d</sup> |

<sup>a</sup> low solubility

<sup>b</sup> recalculated from data determined vs Ag/AgNO<sub>3</sub> using  $E_{\text{Ag/AgNO}_3}^0 = 0.30 \text{ V vs SCE}$

<sup>c</sup> given vs Ferricinium/Ferrocene couple

<sup>d</sup> as reported in literature, i.e. calculated using  $E_{1/2}$  instead of  $E_{\text{onset}}$

### 3.3. Electronic absorption and Raman spectroscopies

The electronic absorption and Raman spectra of the bilayers heterostructures were compared to the respective spectra of thin films of the individual species (Fig. 5). For all the samples, bilayers films spectra appear as the superposition of spectra of the individual species. The electronic absorption spectra of **2** and **3** (Fig. 5b and 5c) show a apparent splitting of Q band, by ca. 90 nm while only one Q band appears for **1** (Fig. 5a). Film spectra of **1** displayed a hypsochromic shift of 47 nm from its solution spectra (Q band centered at 702 nm, [50]), which highlights the formation of H-type aggregates associated with face-to-face intermolecular interactions in the solid state [64]. In the thin film spectra of **2** and **3**, the Q

bands experienced both hypsochromic and bathochromic shifts from their solution spectra (Q band centered at 675 and 691 nm, respectively, Fig. S1), indicating the existence of H-type aggregates and J-type aggregates associated with both face-to-face and edge-to-edge intermolecular interactions in the solid state [65]. All these spectra display a band at ca. 470 nm, which has contribution from the sublayer as well as from the radical nature of LuPc<sub>2</sub> [66]. There is no additional band at higher wavelengths, indicating the absence of significant charge transfer between the two layers, as described previously for Cu(F<sub>16</sub>Pc)/LuPc<sub>2</sub> heterostructure [67].

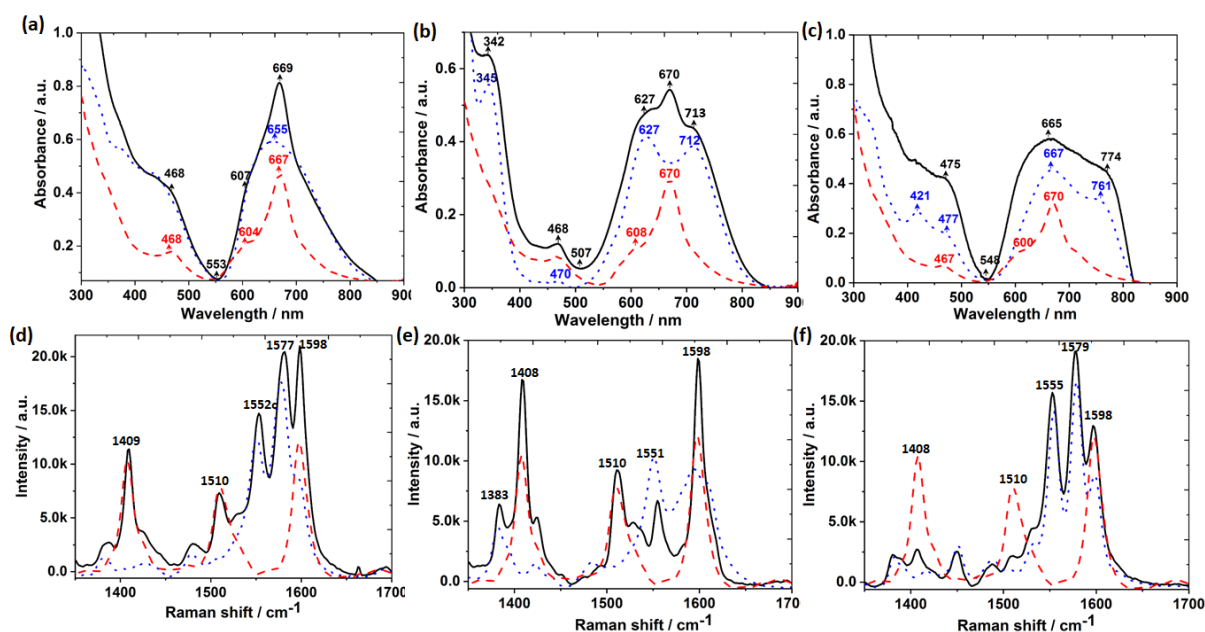


**Figure 5.** UV-vis electronic absorption spectra (a, b, c) and Raman spectra (d, e, f) of the bilayer films of **1**/LuPc<sub>2</sub>, **2**/LuPc<sub>2</sub> and **3**/LuPc<sub>2</sub> on glass, respectively. Red, blue and black color correspond to spectra of LuPc<sub>2</sub>, sublayer and the bilayer, respectively.

The Raman spectra of the bilayer heterostructures and individual phthalocyanines in them coated on glass substrate were recorded between 500 and 1700 cm<sup>-1</sup>. The comparison of enlarged spectra in 1350-1700 cm<sup>-1</sup> range (Fig. 5d-f) display the characteristics Raman peaks of each phthalocyanines in the bilayer, confirming the presence of both MPc materials in the heterostructure films. In the shown region, the three main peaks of LuPc<sub>2</sub> are visible on the

bilayer films at  $1409\text{ cm}^{-1}$  assigned to isoindole stretching,  $1510\text{ cm}^{-1}$  to C=C pyrrole stretching, and  $1598\text{ cm}^{-1}$  associated with benzene stretching, out of which the last one is common to all MPc. In each bilayer spectra, footprint of sublayers can be noticed, for example at  $1552$  and  $1577\text{ cm}^{-1}$  for **1**, at  $1383$  and  $1551\text{ cm}^{-1}$  for **2** and at  $1555$  and  $1579\text{ cm}^{-1}$  for **3**, all attributed to benzene stretching except at  $1383\text{ cm}^{-1}$  [68]. The full Raman spectra of **1-3** and LuPc<sub>2</sub> are given in supplementary information (Fig. S5).

### 3.4. Electrical characterizations of organic heterojunction device

The I(V) curves of the 50 nm thick films of **1**, **2** and **3** coated on ITO interdigitated electrodes patterned glass substrate were recorded as a function of bias voltage in the range of -10 V to 10 V (Fig. S6). The films were highly resistive, as expected for monocyclic phthalocyanines substituted with non-conjugated organic moieties, exhibiting a noisy I(V) curves and current at 10 V of ca. 0.1 nA, corresponding to a conductivity in the range  $10^{-9} - 10^{-10}\text{ }\Omega^{-1}\text{cm}^{-1}$ . Such a low conductivity of these MPc materials makes them suitable for building a MSDI type organic heterojunctions, by combining with a higher conducting organic semiconductor like LuPc<sub>2</sub>. The similar I(V) curves of MSDI device having sublayer among **1**, **2** and **3** and LuPc<sub>2</sub> as top layer display a symmetrical and non-linear characteristics, and much higher conductivity such that current at +10 V are 600, 80 and 5  $\mu\text{A}$ , for **1**, **2** and **3** – based heterojunctions, respectively (Fig. 6a–c). It is evident that symmetric octa-substitution of hexyl sulfanyl groups in the sublayer MPc leads to the highest conducting MSDI device whereas the unsymmetrical MPc **3** leads to the lowest conducting MSDI. It is interesting to note that although chemiresistors based on **1**, **2**, **3** showed almost similar current in the studied bias range, a huge difference can be observed for related MSDI. Such a huge enhancement in the MSDI devices current is attributed to the organic heterojunction effects in which mobile charges are accumulated at the interface because of workfunction ( $\Phi$ ) difference between LuPc<sub>2</sub> and **1**, **2** and **3** [31,37]. Accumulation of  $e^-$  and  $h^+$  at the interface fills the traps and

facilitate the faster mobility of charges making the interface highly conducting. Noteworthy is that such interfacial alignments of  $e^-$  and  $h^+$  are affected by the electronic effects of substituents in the sublayer MPc, which is also evident on the observed I(V) curves. Based on the  $\Phi$  of **1**, **2** and **3** and LuPc<sub>2</sub>, accumulation/depletion and accumulation heterojunction are formed as depicted in Fig. 6d–f. Notably, **1**/LuPc<sub>2</sub> and **3**/LuPc<sub>2</sub> forms accumulation/depletion heterojunction because the presence of electron donating hexyl-sulfanyl groups in **1** and **3** make them electron rich (and  $\Phi_{\mathbf{1\ or\ 3}} < \Phi_{\text{LuPc}_2}$ ), facilitating  $e^-$  injection into the p-type LuPc<sub>2</sub> layer. Consequently,  $h^+$  carriers are depleted (because of  $e^-$  and  $h^+$  recombination) in LuPc<sub>2</sub> layer and created in the respective sublayer close to the interface. However, charges accumulation and depletion at the interface are higher in **1**/LuPc<sub>2</sub> compared to **3**/LuPc<sub>2</sub>, which also explains its more than 100 times higher current in the I(V) curves. On the other hand, because of the presence of eight strong electron withdrawing hexyl-sulfonyl groups, **2** is electron deficient (and  $\Phi_{\mathbf{2}} > \Phi_{\text{LuPc}_2}$ ), which enables  $e^-$  injection from LuPc<sub>2</sub> to the sublayer, as a result of these electrons and holes are accumulated in the sublayer and LuPc<sub>2</sub>, respectively. The detailed mechanism of these heterojunction formations was discussed in our recent works [37,46]. The non-linearity in the I(V) curves is also attributed to the heterojunction formation, which represents the energy barrier experienced by the mobile carriers to overcome the bulk transport and start the interfacial transport. The apparent energy barrier ( $U_{\text{th}}$ ) is determined by taking a tangent to the I(V) curves at higher bias, the x-intercept of which denotes the  $U_{\text{th}}$ . Thus, for **1**/LuPc<sub>2</sub>, **2**/LuPc<sub>2</sub> and **3**/LuPc<sub>2</sub> heterojunctions,  $U_{\text{th}}$  values of 3.35, 2.86 and 2.69 V were determined, respectively.

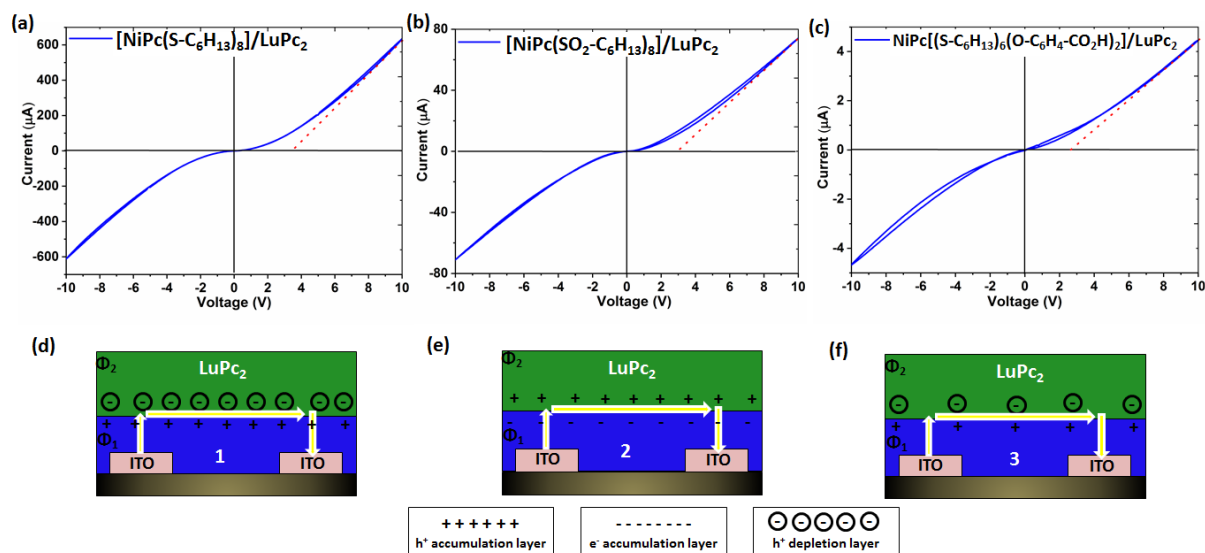


**Figure 6.** Current-voltage characteristics of **1**/LuPc<sub>2</sub> (a), **2**/LuPc<sub>2</sub> (b) and **3**/LuPc<sub>2</sub> (c) heterojunctions in a bias range -10 V to 10 V. Respective charge transfer pathways at the interface of **X**/LuPc<sub>2</sub> heterojunctions, **X** = **1**, **2** and **3**.

### 3.5. Chemosensing properties towards NH<sub>3</sub>

The sensing properties of different heterojunctions devices were investigated at first by exposing to 90 ppm of NH<sub>3</sub> with 10 min/40 min exposure/recovery cycles, respectively, at room temperature. As depicted in Fig. 7a-c, the response is negative (decrease in device current in the exposure cycle) for **1**/LuPc<sub>2</sub> and **3**/LuPc<sub>2</sub> while positive (increase in device current in the exposure cycle) for **2**/LuPc<sub>2</sub> towards NH<sub>3</sub>, indicating the p-type nature of the former two and n-type behavior of the latter heterojunction device, taking into account electron donating nature of the exposed gas. Owing to the presence of electron donating hexyl-sulfanyl groups in **1** and **3**, and electron accepting hexyl-sulfonyl groups in **2**, p-type and n-type semiconducting polarity, respectively, was expected, which we report it for the first time. Moreover, n-type MPC materials are usually obtained by substituting very strong acceptors like -NO<sub>2</sub>, -CN and -F moieties, but here we demonstrate that air stable n-type semiconductor can be also obtained by a relatively moderate electron acceptor like -SO<sub>2</sub>R.

The sensors responses can also be correlated with the different types of heterojunctions shown in Fig. 5d-f, based on mechanism proposed in our recent works [46]. Accordingly, for **1**/LuPc<sub>2</sub> and **3**/LuPc<sub>2</sub> device, upon e<sup>-</sup> doping from NH<sub>3</sub> on the sensor top surface,  $\Phi_{\text{LuPc}_2}$  is decreased, reducing the e<sup>-</sup> injection from sublayer and also the effective h<sup>+</sup> concentration at the interface in the sublayer, which is manifested by the decrease in device current during exposure cycle. On the contrary in accumulation heterojunction in **2**/LuPc<sub>2</sub> device, decrease in  $\Phi_{\text{LuPc}_2}$  upon NH<sub>3</sub> exposure increases its e<sup>-</sup> donating ability to the sublayer, therefore e<sup>-</sup> concentration at the interface in the sublayer increases, which is also observed as positive response of the sensor. Notably, sensor based on **1**/LuPc<sub>2</sub> exhibited the highest and most stable response as exposure and recovery currents are similar for different cycles. On the other hand, a relatively lower and unstable responses are noticed for **2**/LuPc<sub>2</sub> and **3**/LuPc<sub>2</sub> highlighted by decreasing device current with repeated exposure/recovery cycles, which can be attributed to diffusion or irreversible adsorption of NH<sub>3</sub> on the sensors film. The relative response (RR), defined as  $RR = (I_f - I_0)/I_0$ , I<sub>0</sub> and I<sub>f</sub> being the current values at the beginning and the end of the exposure period, respectively, allows a quantitative evaluation of the sensors response. The calculated RR values were -7.7% and -30% for **1**/LuPc<sub>2</sub> and **3**/LuPc<sub>2</sub>, respectively, and +4.3% for **2**/LuPc<sub>2</sub>. It should be noted however that higher RR of **3**/LuPc<sub>2</sub> is mainly attributed to comparatively low baseline current I<sub>0</sub>.

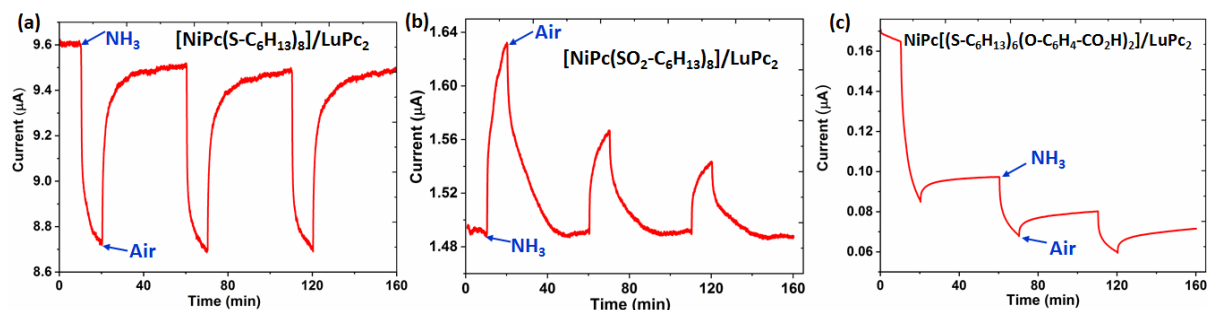


**Figure 7.** Current response of **1/LuPc<sub>2</sub>** (a), **2/LuPc<sub>2</sub>** (b) and **3/LuPc<sub>2</sub>** (c) heterojunctions to 90 ppm ammonia, during exposure/recovery cycles (10 min/40 min), at 30% relative humidity, with a bias of 1 V.

The sensing properties of different MSDI devices were also studied during short exposure/recovery cycles (1 min/4 min) in 10-90 ppm NH<sub>3</sub> concentration range. The sensors current as a function of time has been shown in Fig. 8a–c for 5 exposure/recovery cycles at each concentration in decreasing and increasing modes. A stable baseline and good repeatability of response at 5 different cycles for a given NH<sub>3</sub> concentration in **1/LuPc<sub>2</sub>** and **3/LuPc<sub>2</sub>** is noted, while **2/LuPc<sub>2</sub>** device shows relatively noisy signal and poor repeatability. Moreover, responses are similar at a given concentration in an increasing and decreasing mode for **1/LuPc<sub>2</sub>** and **3/LuPc<sub>2</sub>**, but a hysteresis is noted for **2/LuPc<sub>2</sub>**. Interestingly, for **2/LuPc<sub>2</sub>** and **3/LuPc<sub>2</sub>**, reversible sensor response is obtained at short exposure/recovery cycles contrary to irreversible behavior noted for longer exposure/recovery times, indicating the negligible contribution of diffusion or irreversible adsorption when sensor surface is exposed for a small time to NH<sub>3</sub>. The RR associated with these response curves were determined and are plotted as a function of NH<sub>3</sub> concentration as shown in Fig. 8d-f. The RR values at 10 ppm of NH<sub>3</sub> are estimated as -1.8 %, 0.6 % and -3.6 % for **1/LuPc<sub>2</sub>**, **2/LuPc<sub>2</sub>** and **3/LuPc<sub>2</sub>**, respectively, making them suitable to detect NH<sub>3</sub> below the mandated international guidelines (OSHA permissible exposure limit; 50 ppm, European air quality labor legislation for NH<sub>3</sub> sets a daily exposure limit at 20 ppm). It can be also noted that all the three sensors exhibited non-linear calibration curves in the studied NH<sub>3</sub> concentration range, such that responses tend to saturate at higher concentration. Such kind of behavior is typical for NH<sub>3</sub> sensors, also reported previously[69]. These response curves also indicate a Langmuir type adsorption in gas-material interaction, in which the competition among gas molecules for the active sites at higher concentration lowers the sensor response [70].

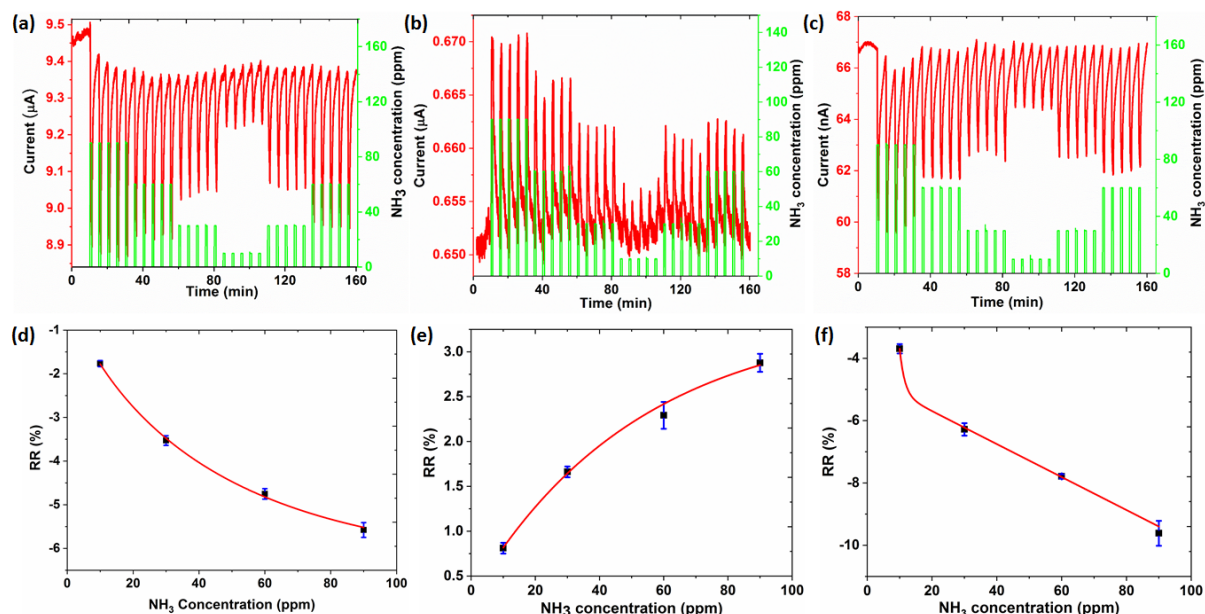


**Figure 8.** Current response of **1/LuPc<sub>2</sub>** (a), **2/LuPc<sub>2</sub>** (b) and **3/LuPc<sub>2</sub>** (c) heterojunctions to NH<sub>3</sub>, in the range 10-90 ppm, during exposure/recovery cycles (1 min/4 min), at 30% rh, with a bias of 1 V. RR of **1/LuPc<sub>2</sub>** (d), **2/LuPc<sub>2</sub>** (e) and **3/LuPc<sub>2</sub>** (f) heterojunctions as a function of NH<sub>3</sub> concentration.

Humidity presents the main interference in the selective detection of NH<sub>3</sub> in majority of the real applications, therefore the sensors response was investigated at different rh in the range of 10–70 % at a fixed NH<sub>3</sub> concentration of 30 ppm. The variations in current as a function of time at different rh levels have been shown in Fig. 9 for **1/LuPc<sub>2</sub>** and **3/LuPc<sub>2</sub>** devices submitted to alternate exposure/recovery cycles to NH<sub>3</sub>. It is evident from these responses that both the sensors are sensitive towards humidity but in a different way. The effect of rh change from 10% to 30% is minimal on the baseline as well as RR of sensors. But for rh change from 50% to 70%, a sudden decrease (by ca. 17%) and an enhancement (by ca. 20%) in baseline current is noted for **1/LuPc<sub>2</sub>** and **3/LuPc<sub>2</sub>** devices, respectively. The influence of rh variations on RR of the sensors is also noted as for **1/LuPc<sub>2</sub>**, the absolute value of RR increases by 15%, 20% and 40% for the rh change from 10 to 30%, 30 to 50% and 50 to 70%, respectively. However, the absolute RR values remain unaffected at lower concentrations (20 ppm and 10 ppm) for a similar variation in rh (Fig. S7). Moreover, the

process is reversible as exhibited by the return of the baseline to its initial level, while rapidly changing the rh value from 70% to 10%. For **3**/LuPc<sub>2</sub>, the RR value remains unchanged between 10 and 30% rh, while it decreases by 10% from 30 to 50% of rh and at higher rh it shows inversion of response from negative to positive. Such unique effect displayed by the sensor can be associated with change of semiconducting polarity of **3**/LuPc<sub>2</sub> heterojunction from p-type to n-type. Thus, **3**/LuPc<sub>2</sub> device exhibits ambipolar transport characterized by the presence of near equilibrium concentration of e<sup>-</sup> and h<sup>+</sup> carriers. The application of higher rh acts as a trigger to shift the equilibrium towards the one dominated by e<sup>-</sup>, reverting the p-type behavior into n-type and thus positive response towards ammonia, as we reported for the first time with the octafluoro copper phthalocyanine as a sublayer [71]. Accordingly, extended exposure at high rh can induce slow diffusion of water and NH<sub>3</sub> in the heterojunction sublayer, which can donate e<sup>-</sup> there and shifts the balance of ambipolarity from p-type to n-type. Meanwhile, the RR absolute value increased by one third for a change of rh from 10 to 70%. Effect of rh was also studied for **2**/LuPc<sub>2</sub> device, which showed a very high sensitivity to rh variations (Fig. S8), and apparently sensitivity towards NH<sub>3</sub> disappeared after 50% of rh.

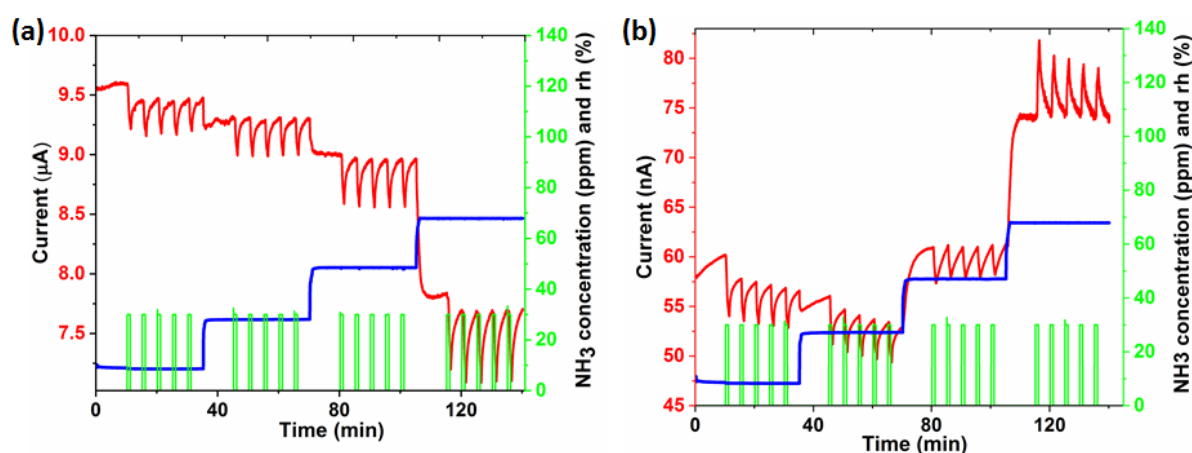


**Figure 9.** Current response of **1**/LuPc<sub>2</sub> (a) and **3**/LuPc<sub>2</sub> (b) heterojunctions to 30 ppm ammonia, during exposure/recovery cycles (1 min/4 min), with a bias of 1 V, in the range 10-70 % rh.

Long term stability of the **1**/LuPc<sub>2</sub> sensor was evaluated by performing measurements after 18 months of storage in ambient atmosphere in the dark. The I(V) curves as shown in Fig. S9a is stable and yielded very similar potential barrier ( $U_{th}$ ) of 3.25 V as obtained for a new sample (3.35 V). Sensor responses for long as well as short exposure/recovery cycles are also very stable (Fig. S9b and S9c). Moreover, the sensor calibration curve shows a similar non-linear variation as a function of NH<sub>3</sub> concentration, as noted for a new sample. However, a decrease in the sensor baseline current as well as RR at different concentrations is noted as compared to new sample. This ageing effect can be attributed to the chemisorption of water molecules or molecular oxygen over extended period of storage in atmospheric conditions, which can be minimized using a suitable packaging that lower the exposure to oxygen.

## Conclusion

In summary, we demonstrated the electronic effects of substituents in tuning the electrical properties of phthalocyanines based organic heterostructures, which are subsequently exploited to develop a sensitive and selective ammonia sensor. A set of octasubstituted NiPc with electron donating hexyl-sulfanyl, electron accepting hexyl sulfonyl and a combination of 6 hexyl-sulfanyl and 2 moderately electron-accepting *p*-carboxyphenoxy groups are successfully synthesized. The synthesized NiPc derivatives exhibited characteristics UV-vis, NMR, FT-IR and mass spectral peaks associated with structure and functional groups of each molecule, confirming their chemical purity and molecular structure. The electrochemical studies by CV further confirmed the electronic nature of the substituent in **1**, **2** and **3** as electron donating, accepting and moderate accepting. These materials are incorporated into MSDI heterojunction devices by solution processing as a sublayer in combination with vacuum deposited LuPc<sub>2</sub> as top layer. The UV-vis and Raman spectra of different bilayer

heterostructures displayed a superposition of thin film spectra of individual layer, confirming successful integration of both materials in the MSDI device. The I(V) characteristics of different MSDI heterojunction revealed a symmetric and non-linear behavior, attributed to the formation of energy barriers at the interface of the heterostructure, which is identified as accumulation or accumulation/depletion heterojunction depending on the workfunction of each material in the MSDI device. These devices exhibited positive as well as negative response towards ammonia depending on the electronic effects of substituents in the sublayer NiPc, such that **1**/LuPc<sub>2</sub> and **3**/LuPc<sub>2</sub> displayed negative while **2**/LuPc<sub>2</sub> showed positive responses. Among the three sensors, **1**/LuPc<sub>2</sub> revealed the best sensing properties indicated by high repeatability in RR and stable baseline signal and could detect NH<sub>3</sub> concentration below the mandated international guidelines. The variation of humidity exhibited low interference on the sensors baseline as well as RR up to rh value of 50%. However, higher humidity affected sensor baseline and also inverted the negative response of **3**/LuPc<sub>2</sub> into positive one, demonstrating as trigger of ambipolar transport in **3**/LuPc<sub>2</sub> MSDI. This is one of the rare examples of ambipolar gas sensors reported so far [47].

#### **4. ACKNOWLEDGMENTS**

The Scientific and Technological Research Council of Turkey (TUBITAK) and the French Embassy in Turkey are gratefully acknowledged for the bilateral Partenariat Hubert Curien between Turkey and France (project PHC-Bosphorus 117Z623 / 39745WG). The authors are thankful to *Agence Nationale de la Recherche* for a generous funding throughout the project (OUTSMART ANR-2015-CE39-0004-03). Authors would also like to thank European Union and *Conseil Régional de Bourgogne* for providing financial support through the FABER and the PARI SMT 08 and CDEA programs. Authors thank SATT SAYENS for supporting the analytical platform (PACSMUB) at ICMUB. Dr. Vaibhav Vibhu (Forschungszentrum Jülich, Germany) is thanked for SEM and EDS analyses of LuPc<sub>2</sub> thin films. This work was

supported by the PIA-Excellence ISITE-BFC (CoMICS program 2019-2022 : Chemistry of Molecular Interactions - Catalysis and Sensors) (A. K.). The Ministère de la Cohésion des Territoires et des Relations avec les Collectivités Territoriales (France) and the *Conseil Régional de Bourgogne* are thanked for the CPER.

### **ORCID**

Marcel Bouvet: 0000-0002-2272-6633

Fabienne Dumoulin: 0000-0002-0388-8338

Ümit İşci: 0000-0002-6285-0524

Abhishek Kumar: 0000-0002-4306-9644

Rita Meunier-Prest: 0000-0001-5597-3879

Zeynel Şahin: 0000-0002-7719-7652

### **Author Contributions**

The manuscript was written through contributions of all authors. All authors have given approval to the final version of the manuscript.

## References

- [1] N. Yamazoe, K. Shimano, Fundamentals of semiconductor gas sensors, in: *Semiconductor Gas Sensors*, Woodhead Publishing, 2020: pp. 3–38. doi:10.1016/B978-0-08-102559-8.00001-X.
- [2] N. Barsan, M. Huebner, U. Weimar, Conduction mechanism in semiconducting metal oxide sensing films: impact on transduction, in: *Semiconductor Gas Sensors*, Woodhead Publishing, 2020: pp. 39–69. doi:10.1016/B978-0-08-102559-8.00002-1.
- [3] H. Ji, W. Zeng, Y. Li, Gas sensing mechanisms of metal oxide semiconductors: a focus review, *Nanoscale*. 11 (2019) 22664–22684. doi:10.1039/C9NR07699A.
- [4] A. Dey, Semiconductor metal oxide gas sensors: A review, *Mater. Sci. Eng., B*. 229 (2018) 206–217. doi:10.1016/j.mseb.2017.12.036.
- [5] T. Li, W. Zeng, Z. Wang, Quasi-one-dimensional metal-oxide-based heterostructural gas-sensing materials: A review, *Sens. Actuators: B. Chem.* 221 (2015) 1570–1585. doi:10.1016/j.snb.2015.08.003.
- [6] G.F. Fine, L.M. Cavanagh, A. Afonja, R. Binions, Metal oxide semi-conductor gas sensors in environmental monitoring, *Sensors*. 10 (2010) 5469–5502. doi:10.3390/s100605469.
- [7] Y.-F. Sun, S.-B. Liu, F.-L. Meng, J.-Y. Liu, Z. Jin, L.-T. Kong, et al., Metal oxide nanostructures and their gas sensing properties: A review, *Sensors*. 12 (2012) 2610–2631. doi:10.3390/s120302610.
- [8] K. Wetchakun, T. Samerjai, N. Tamaekong, C. Liewhiran, C. Siriwong, V. Kruefu, et al., Semiconducting metal oxides as sensors for environmentally hazardous gases, *Sens. Actuators: B. Chem.* 160 (2011) 580–591. doi:10.1016/j.snb.2011.08.032.
- [9] H.-J. Kim, J.-H. Lee, Highly sensitive and selective gas sensors using p-type oxide semiconductors: Overview, *Sens. Actuators: B. Chem.* 192 (2014) 607–627. doi:10.1016/j.snb.2013.11.005.
- [10] C. Zhang, A. Boudiba, P. De Marco, R. Snyders, M.-G. Olivier, M. Debligny, Room temperature responses of visible-light illuminated WO<sub>3</sub> sensors to NO<sub>2</sub> in sub-ppm range, *Sens. Actuators: B. Chem.* 181 (2013) 395–401. doi:10.1016/j.snb.2013.01.082.
- [11] S. Jain, A. Patrike, S.S. Badadhe, M. Bhardwaj, S. Ogale, Room-temperature ammonia gas sensing using mixed-valent CuCo<sub>2</sub>O<sub>4</sub> nanoplatelets: Performance enhancement through stoichiometry control, *ACS Omega*. 3 (2018) 1977–1982. doi:10.1021/acsomega.7b01958.
- [12] T. Becker, L. Tomasi, C. Bosch-v Braunmühl, G. Müller, G. Sberveglieri, G. Fagli, et al., Ozone detection using low-power-consumption metal-oxide gas sensors, *Sens. Actuators a: Phys.* 74 (1999) 229–232. doi:10.1016/S0924-4247(98)00301-X.
- [13] J. Nisar, Z. Topalian, A. De Sarkar, L. Österlund, R. Ahuja, TiO<sub>2</sub>-based gas sensor: a possible application to SO<sub>2</sub>, *ACS Appl. Mater. Interfaces*. 5 (2013) 8516–8522. doi: [10.1021/am4018835](https://doi.org/10.1021/am4018835)
- [14] A. Mirzaei, S.S. Kim, H.W. Kim, Resistance-based H<sub>2</sub>S gas sensors using metal oxide nanostructures: A review of recent advances, *Journal of Hazardous Materials*. 357 (2018) 314–331. doi:10.1016/j.jhazmat.2018.06.015.
- [15] U. Hofer, J. Frank, M. Fleischer, High temperature Ga<sub>2</sub>O<sub>3</sub>-gas sensors and SnO<sub>2</sub>-gas sensors: a comparison, *Sens. Actuators: B. Chem.* 78 (2001) 6–11. doi:10.1016/S0925-4005(01)00784-5.
- [16] R. Song, Z. Wang, X. Zhou, L. Huang, L. Chi, Gas- sensing performance and operation mechanism of organic  $\pi$ - conjugated materials, *ChemPlusChem*. 84 (2019) 1222–1234. doi:10.1002/cplu.201900277.

- [17] B. Bott, T.A. Jones, A highly sensitive NO<sub>2</sub> sensor based on electrical conductivity changes in phthalocyanine films, *Sens. Actuators*. 5 (1984) 43–53. doi:10.1016/0250-6874(84)87005-5.
- [18] T.A. Jones, B. Bott, S.C. Thorpe, Fast response metal phthalocyanine-based gas sensors, *Sens. Actuators*. 17 (1989) 467–474. doi: [10.1016/0250-6874\(89\)80033-2](https://doi.org/10.1016/0250-6874(89)80033-2)
- [19] F.I. Bohrer, C.N. Colesniuc, J. Park, M.E. Ruidiaz, I.K. Schuller, A.C. Kummel, et al., Comparative gas sensing in cobalt, nickel, copper, zinc, and metal-free phthalocyanine chemiresistors, *J. Am. Chem. Soc.* 131 (2009) 478–485. doi:10.1021/ja803531r.
- [20] F.I. Bohrer, A. Sharoni, C. Colesniuc, J. Park, I.K. Schuller, A.C. Kummel, et al., Gas sensing mechanism in chemiresistive cobalt and metal-free phthalocyanine thin films, *J. Am. Chem. Soc.* 129 (2007) 5640–5646. doi:10.1021/ja0689379.
- [21] D. Klyamer, A. Sukhikh, S. Gromilov, P. Krasnov, T. Basova, Fluorinated metal phthalocyanines: Interplay between fluorination degree, films orientation, and ammonia sensing properties, *Sensors*. 18 (2018) 2141. doi:10.3390/s18072141.
- [22] G. Guillaud, J. Simon, J.P. Germain, Metallophthalocyanines: Gas sensors, resistors and field effect transistors, *Coord. Chem. Rev.* 178-180 (1998) 1433–1484. doi:10.1016/S0010-8545(98)00177-5.
- [23] J.H. Park, J.E. Royer, E. Chagarov, T. Kaufman-Osborn, M. Edmonds, T. Kent, et al., Atomic imaging of the irreversible sensing mechanism of NO<sub>2</sub> adsorption on copper phthalocyanine, *J. Am. Chem. Soc.* 135 (2013) 14600–14609. doi:10.1021/ja403752r.
- [24] M. Bouvet, E.A. Silinsh, J. Simon, Determination of energy gap values in molecular crystals II. Intrinsic dark conductivity and electrochemical methods, *Mol. Mater.* 5 (1995) 255–277.
- [25] V. Rani, A. Sharma, P. Kumar, B. Singh, S. Ghosh, Charge transport mechanism in copper phthalocyanine thin films with and without traps, *RSC Advances*. 7 (2017) 54911–54919. doi: 10.1039/c7ra08316e
- [26] J.T.E. Quinn, J. Zhu, X. Li, J. Wang, Y. Li, Recent progress in the development of n-type organic semiconductors for organic field effect transistors, *J. Mater. Chem. C*. 5 (2017) 8654–8681. doi:10.1039/C7TC01680H.
- [27] J. Brunet, V. Parra Garcia, A. Pauly, C. Varenne, B. Lauron, An optimised gas sensor microsystem for accurate and real-time measurement of nitrogen dioxide at ppb level, *Sens. Actuators: B. Chem.* 134 (2008) 632–639. doi:10.1016/j.snb.2008.06.010.
- [28] S. Ji, H. Wang, T. Wang, D. Yan, A High- Performance Room- Temperature NO<sub>2</sub> Sensor Based on An Ultrathin Heterojunction Film, *Adv. Mater.* 25 (2013) 1755–1760. doi:10.1002/adma.201204134.
- [29] T. Shaymurat, Q. Tang, Y. Tong, L. Dong, Y. Liu, Gas Dielectric transistor of CuPc single crystalline nanowire for SO<sub>2</sub> detection down to sub- ppm levels at room temperature, *Adv. Mater.* 25 (2013) 2269–2273. doi:10.1002/adma.201204509.
- [30] D. Yan, H. Wang, B. Du, *Introduction to Organic Semiconductor Heterojunctions*, John Wiley & Sons, 2010.
- [31] H. Wang, D. Yan, Organic heterostructures in organic field-effect transistors, *NPG Asia Mater.* 2 (2010) 69–78. doi:10.1038/asiamat.2010.44.
- [32] Y. Zhao, Y. Guo, Y. Liu, 25th Anniversary article: Recent advances in n-type and ambipolar organic field-effect transistors, *Adv. Mater.* 25 (2013) 5372–5391. doi:10.1002/adma.201302315.
- [33] R. Murdey, N. Sato, M. Bouvet, Frontier electronic structures in fluorinated copper phthalocyanine thin films studied using ultraviolet and inverse photoemission spectroscopies, *Mol. Cryst. Liq. Cryst.* 455 (2006) 211–218. doi:10.1080/15421400600698469.

- [34] R. Murdey, M. Bouvet, M. Sumimoto, S. Sakaki, N. Sato, Direct observation of the energy gap in lutetium bisphthalocyanine thin films, *Synth. Met.* 159 (2009) 1677–1681. doi:10.1016/j.synthmet.2009.05.002.
- [35] H. Brinkmann, C. Kelting, S. Makarov, O. Tsaryova, G. Schnurpfeil, D. Wöhrle, et al., Fluorinated phthalocyanines as molecular semiconductor thin films, *Phys. Status Solidi A.* 205 (2008) 409–420. doi:10.1002/pssa.200723391.
- [36] J.P. Meyer, D. Schlettwein, Influence of central metal and ligand system on conduction type and charge carrier transport in phthalocyanine thin films, *Adv. Mater. Opt. Electr.* 6 (1996) 239–244. doi:10.1002/(SICI)1099-0712(199609)6:5/6<239::AID-AMO274>3.0.CO;2-E.
- [37] A. Kumar, R. Meunier-Prest, M. Bouvet, Organic heterojunction devices based on phthalocyanines: A new approach to gas chemosensing, *Sensors.* 20 (2020) 4700. doi:10.3390/s20174700
- [38] S. Han, J. Cheng, H. Fan, J. Yu, L. Li, Achievement of high-response organic field-effect transistor NO<sub>2</sub> sensor by using the synergistic effect of ZnO/PMMA hybrid dielectric and CuPc/Pentacene heterojunction, *Sensors.* 16 (2016) 1763. doi:10.3390/s16101763.
- [39] W. Huang, K. Besar, R. LeCover, A.M. Rule, P.N. Breyse, H.E. Katz, Highly sensitive NH<sub>3</sub> detection based on organic field-effect transistors with tris(pentafluorophenyl)borane as receptor, *J. Am. Chem. Soc.* 134 (2012) 14650–14653. doi:10.1021/ja305287p.
- [40] X. Wang, S. Ji, H. Wang, D. Yan, Highly sensitive gas sensor enhanced by tuning the surface potential, *Org. Electron.* 12 (2011) 2230–2235. doi:10.1016/j.orgel.2011.09.014.
- [41] V. Parra, M. Bouvet, Semiconductor transducer and its use in a sensor for detecting electron-donor or electron-acceptor species, US8450725 B2, 2013.
- [42] V. Parra, J. Brunet, A. Pauly, M. Bouvet, Molecular semiconductor-doped insulator (MSDI) heterojunctions: an alternative transducer for gas chemosensing, *Analyst.* 134 (2009) 1776–1778. doi:10.1039/b906786h.
- [43] D.R. Miller, S.A. Akbar, P.A. Morris, Nanoscale metal oxide-based heterojunctions for gas sensing: A review, *Sens. Actuators: B. Chem.* 204 (2014) 250–272. doi:10.1016/j.snb.2014.07.074.
- [44] F.E. Annanouch, Z. Haddi, S. Vallejos, P. Umek, P. Guttman, C. Bittencourt, et al., Aerosol-assisted CVD-grown WO<sub>3</sub> nanoneedles decorated with copper oxide nanoparticles for the selective and humidity-resilient detection of H<sub>2</sub>S, *ACS Appl. Mater. Interfaces.* 7 (2015) 6842–6851. doi:10.1021/acsami.5b00411.
- [45] M. Mateos, R. Meunier-Prest, J.-M. Suisse, M. Bouvet, Modulation of the organic heterojunction behavior, from electrografting to enhanced sensing properties, *Sens. Actuators: B. Chem.* 299 (2019) 126968. doi.org/10.1016/j.snb.2019.126968
- [46] S. Ouedraogo, R. Meunier-Prest, A. Kumar, M. Bayo-Bangoura, M. Bouvet, Modulating the Electrical Properties of Organic Heterojunction Devices Based On Phthalocyanines for Ambipolar Sensors, *ACS Sens.* 5 (2020) 1849–1857. doi:10.1021/acssensors.0c00877.
- [47] M. Bouvet, S. Ouedraogo, R. Meunier-Prest, Ambipolar materials for gas sensors, in: Y. Zhou, S.T. Han (Eds.), *Ambipolar Materials and Devices*, 2020. doi.org/10.1039/9781788019279
- [48] H. Kwon, H. Yoo, M. Nakano, K. Takimiya, J.-J. Kim, J.K. Kim, Gate-tunable gas sensing behaviors in air-stable ambipolar organic thin-film transistors, *RSC Advances.* 10 (2020) 1910–1916. doi:10.1039/C9RA09195E.

- [49] A.G. Gürek, Ö. Bekaroglu, Octakis(alkylthio)-substituted phthalocyanines and their interactions with silver( I ) and palladium( II ) ions, *J. Chem. Soc., Dalton Trans.* 0 (1994) 1419–1423. doi:10.1039/DT9940001419.
- [50] U. Işci, A.S. Faponle, P. Afanasiev, F. Albrieux, V. Briois, V. Ahsen, et al., Site-selective formation of an iron( iv )–oxo species at the more electron-rich iron atom of heteroleptic  $\mu$ -nitrido diiron phthalocyanines, *Chem. Sci.* 6 (2015) 5063–5075. doi:10.1039/C5SC01811K.
- [51] D. Wöhrle, M. Eskes, K. Shigehara, A. Yamada, A Simple Synthesis of 4,5-Disubstituted 1,2-Dicyanobenzenes and 2,3,9,10,16,17,23,24-Octasubstituted Phthalocyanines, *Synthesis.* (1993) 194–196. doi:10.1055/s-1993-25825.
- [52] C. Clarisse, M.-T. Riou, Synthesis and characterization of some lanthanide phthalocyanines, *Inorg. Chim. Acta.* 130 (1987) 139–144. doi:10.1016/S0020-1693(00)85943-5.
- [53] P. Gaudillat, A. Wannebroucq, J.-M. Suisse, M. Bouvet, Bias and humidity effects on the ammonia sensing of perylene derivative/lutetium bisphthalocyanine MSDI heterojunctions, *Sens. Actuators: B. Chem.* 222 (2016) 910–917. doi:10.1016/j.snb.2015.09.015.
- [54] G. Guillaud, J. Simon, Transient properties of nickel phthalocyanine thin film transistors, *Chem. Phys. Lett.* 219 (1994) 123–126. doi:10.1016/0009-2614(94)00050-6.
- [55] B. Tylleman, G. Gbabode, C. Amato, C. Buess-Herman, V. Lemaur, J. Cornil, et al., Metal-free phthalocyanines bearing eight alkylsulfonyl substituents: Design, synthesis, electronic structure, and mesomorphism of new electron-deficient mesogens, *Chem. Mater.* 21 (2009) 2789–2797. doi:10.1021/cm900383c.
- [56] J.-J. André, K. Holczer, P. Petit, M.-T. Riou, C. Clarisse, R. Even, et al., Electrical and magnetic properties of thin films and single crystals of bis(phthalocyaninato)lutetium, *Chem. Phys. Lett.* 115 (1985) 463–466. doi:10.1016/0009-2614(85)85171-X.
- [57] M.M. Ahmida, S.H. Eichhorn, Measurements and prediction of electronic properties of discotic liquid crystalline triphenylenes and phthalocyanines, in: 216th ECS Meeting, ECS, 2010: pp. 1–10. doi:10.1149/1.3314449.
- [58] Y. Zhang, P. Ma, P. Zhu, X. Zhang, Y. Gao, D. Qi, et al., 2,3,9,10,16,17,23,24-Octakis(hexylsulfonyl)phthalocyanines with good n-type semiconducting properties. Synthesis, spectroscopic, and electrochemical characteristics, *J. Mater. Chem.* 21 (2011) 6515–6524. doi:10.1039/c1jm10295h.
- [59] C. Hansch, A. Leo, R.W. Taft, A survey of Hammett substituent constants and resonance and field parameters, *Chem. Rev.* 91 (1991) 165–195. doi:10.1021/cr00002a004.
- [60] Y. Chen, D. Li, N. Yuan, J. Gao, R. Gu, G. Lu, et al., Tuning the semiconducting nature of bis(phthalocyaninato) holmium complexes via peripheral substituents, *J. Mater. Chem.* 22 (2012) 22142–22149. doi:10.1039/c2jm35219b.
- [61] J.L. Brédas, R. Silbey, D.S. Boudreaux, R.R. Chance, Chain-length dependence of electronic and electrochemical properties of conjugated systems: polyacetylene, polyphenylene, polythiophene, and polypyrrole, *J. Am. Chem. Soc.* 105 (1983) 6555–6559. doi:10.1021/ja00360a004.
- [62] C.M. Cardona, W. Li, A.E. Kaifer, D. Stockdale, G.C. Bazan, Electrochemical considerations for determining absolute frontier orbital energy levels of conjugated polymers for solar cell applications, *Adv. Mater.* 23 (2011) 2367–2371. doi:10.1002/adma.201004554.
- [63] S.Z. Topal, U. Işci, U. Kumru, D. Atilla, A.G. Gürek, C. Hirel, et al., Modulation of the electronic and spectroscopic properties of Zn(ii) phthalocyanines by their substitution pattern, *Dalton Trans.* 43 (2014) 6897–6908. doi:10.1039/c3dt53410c.

- [64] M. Bayda, F. Dumoulin, G.L. Hug, J. Koput, R. Gorniak, A. Wojcik, Fluorescent H-aggregates of an asymmetrically substituted mono-amino Zn(II) phthalocyanine, *Dalton Trans.* 46 (2017) 1914–1926. doi:10.1039/C6DT02651F.
- [65] Y. Chen, M. Bouvet, T. Sizun, Y. Gao, C. Plassard, E. Lesniewska, et al., Facile approaches to build ordered amphiphilic tris(phthalocyaninato) europium triple-decker complex thin films and their comparative performances in ozone sensing, *Phys. Chem. Chem. Phys.* 12 (2010) 12851–11. doi:10.1039/c0cp00381f.
- [66] D. Markovitsi, T.-H. Tran-Thi, R. Even, J. Simon, Near infrared absorption spectra of lanthanide bis-phthalocyanines, *Chem. Phys. Lett.* 137 (1987) 107–112. doi:10.1016/0009-2614(87)80313-5.
- [67] M. Bouvet, V. Parra, J.-M. Suisse, Molecular semiconductor-doped insulator (MSDI) heterojunctions as new transducers for chemical sensors, *Eur. Phys. J. Appl. Phys.* 56 (2011) 34103–10. doi:10.1051/epjap/2011110220.
- [68] M. Bao, Y. Bian, L. Rintoul, R. Wang, D.P. Arnold, C. Ma, et al., Vibrational spectroscopy of phthalocyanine and naphthalocyanine in sandwich-type (na)phthalocyaninato and porphyrinato rare earth complexes, *Vibr. Spectrosc.* 34 (2004) 283–291. doi:10.1016/j.vibspec.2004.01.002.
- [69] D. Kwak, Y. Lei, R. Maric, Ammonia gas sensors: A comprehensive review, *Talanta.* 204 (2019) 713–730. doi:10.1016/j.talanta.2019.06.034.
- [70] M. Mateos, M.-D. Tchangai, R. Meunier-Prest, O. Heintz, F. Herbst, J.-M. Suisse, et al., Low conductive electrodeposited poly(2,5-dimethoxyaniline) as a key material in a double lateral heterojunction, for sub-ppm ammonia sensing in humid atmosphere, *ACS Sens.* 4 (2019) 740–747. doi:10.1021/acssensors.9b00109.
- [71] A. Wannebroucq, S. Ouedraogo, R. Meunier-Prest, J.-M. Suisse, M. Bayo, M. Bouvet, On the interest of ambipolar materials for gas sensing, *Sens. Actuators: B. Chem.* 258 (2018) 657–664. doi:10.1016/j.snb.2017.11.146.